

Supplementary Information: A Fully Dynamical Description of Time-Resolved Resonant Inelastic X-ray Scattering of Pyrazine

Antonia Freibert,^{1,*} David Mendive-Tapia,² Oriol Vendrell,^{2,†} and Nils Huse¹

¹*Department of Physics, University of Hamburg,
 Luruper Chaussee 149, 22761 Hamburg, Germany*

²*Theoretical Chemistry, Institute of Physical Chemistry,
 Heidelberg University, Im Neuenheimer Feld 229, 69120, Heidelberg, Germany*

I. Model Hamiltonian Parameters

All values and symmetries of the harmonic ground-state vibrational frequencies ω_i , vertical excitation energies $E^{(n)}$, on-diagonal linear intrastate coupling constants $\kappa_i^{(n)}$, off-diagonal linear inter-state coupling constants $\lambda_i^{(nm)}$ as well as on-diagonal bilinear (quadratic) coupling constants $\gamma_i^{(n)}$ as well as the parameters concerning the Morse and quartic potential used in this work are provided in the form of a separate MCTDH operator file. Details on how to read this file can be found in the MCTDH documentation. The most relevant parameters are furthermore listed in Table I, II and III.

TABLE I. Subdivision of all electronic states of the molecular Hamiltonian considered in this work and their corresponding state symmetries and vertical excitation energies $E^{(\alpha)}$ (in eV) at the Franck-Condon point. A linear vibronic coupling model was used for all sub-Hamiltonians where anharmonicity was taken into account for selected modes and states as noted in the last column. All parameters for \mathbf{H}_{v_1} were taken from ref.¹. \mathbf{H}_{v_2} is described using the parameters from ref.² except for a global energy shift of -0.6 eV in order to maintain the energy gap between \mathbf{H}_{v_1} and \mathbf{H}_{v_2} . \mathbf{H}_{c_1} is taken over from ref.² without any adjustment while \mathbf{H}_{c_2} was parameterised within this work.

Sub-Hamiltonian	State	Symmetry	$E^{(\alpha)}$	Anharmonicity
\mathbf{H}_{v_1}	S_0	A_g	0.00	
	S_1	B_{3u}	3.93	
	S_2	A_u	4.45	
	S_3	B_{2u}	4.79	
	S_4	B_{2g}	5.38	
\mathbf{H}_{v_2}	S_5	A_g	6.08	
	S_6	B_{1u}	6.31	
	S_7	B_{1g}	6.42	
	S_8	B_{1g}	6.51	
	S_9	B_{2u}	6.78	
	S_{10}	B_{1u}	6.87	
	S_{11}	B_{3u}	7.06	
	S_{12}	B_{2u}	7.34	
	S_{13}	B_{3g}	7.40	
	S_{14}	A_g	7.44	
	S_{15}	A_u	7.52	
	S_{16}	B_{1u}	7.54	
	S_{17}	B_{1g}	7.75	
	S_{18}	A_u	7.76	
S_{19}	B_{2g}	7.93		
\mathbf{H}_{c_1}	X_1	B_{2g}	402.30	Morse potential for ν_{24}
	X_2	B_{3u}	402.30	Morse potential for ν_{24}
\mathbf{H}_{c_2}	X_3	B_{1g}	405.05	Quartic potential for ν_1 Morse potential for ν_{24}
	X_4	A_u	405.06	Quartic potential for ν_1 Morse potential for ν_{24}

* afreiber@physnet.uni-hamburg.de

† oriol.vendrell@uni-heidelberg.de

TABLE II. Linear intrastate coupling constant $\kappa_i^{(n)}$ values (in eV) for all excited states in \mathbf{H}_{v_1} , \mathbf{H}_{c_1} and \mathbf{H}_{c_2} . All parameters for \mathbf{H}_{v_1} and \mathbf{H}_{c_1} were taken from ref.¹ and², respectively. All parameters for \mathbf{H}_{c_2} were obtained within this work.

State	κ_3	κ_{11}	κ_{15}	κ_{20}	κ_{24}
S_1	-0.081	-0.038	0.117	-0.087	0.022
S_2	-0.168	-0.083	-0.071	-0.465	0.060
S_3	0.128	-0.183	0.045	0.026	0.018
S_4	-0.184	-0.117	0.165	0.172	0.030
X_1	0.027	-0.040	0.056	0.104	
X_2	0.026	-0.040	0.056	0.105	
X_3	0.123	-0.079	-0.124	-0.273	
X_4	0.123	-0.079	-0.124	-0.275	

TABLE III. Linear interstate coupling constants $\lambda_i^{(nm)}$ (in eV) for all excited states in \mathbf{H}_{v_1} , \mathbf{H}_{c_1} and \mathbf{H}_{c_2} . All parameters for \mathbf{H}_{v_1} and \mathbf{H}_{c_1} were taken from ref.¹ and², respectively. All parameters for \mathbf{H}_{c_2} were obtained within this work.

	(S_1, S_2)	(S_1, S_3)	(S_1, S_4)	(S_2, S_3)	(S_2, S_4)	(S_3, S_4)	(X_1, X_2)	(X_3, X_4)
λ_5				0.060				
λ_8				0.053				
λ_7	0.195							
λ_9					0.018			
λ_{10}			0.207				0.087	0.100
λ_{14}			0.090				0.013	0.109
λ_{18}			0.094				0.099	0.021
λ_{22}			0.000				0.030	0.022
λ_{12}						0.044		
λ_{13}						0.044		
λ_{17}						0.072		
λ_{16}	0.065							
λ_{19}	0.219							
λ_{21}	0.020							

II. fs-XANES spectra

Fig. 1 presents simulated differential X-ray absorption spectra disentangled for each individual transition.

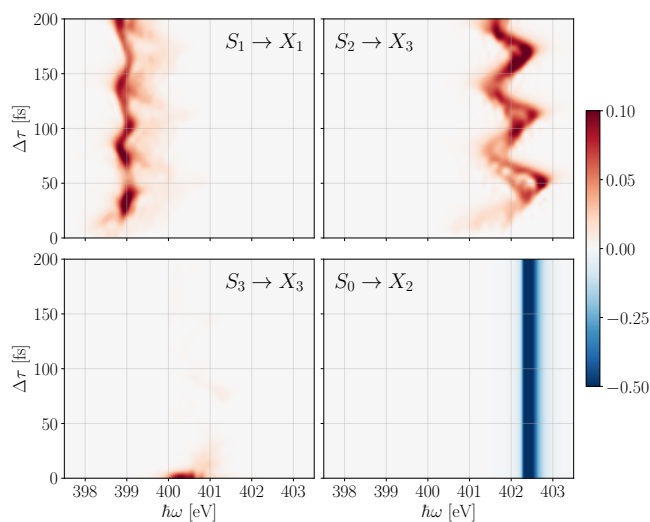


FIG. 1. Three-dimensional map displaying computed fs-XANES spectra for each individual transition.

III. Time Evolution of fs-RIXS spectra

Fig. 2 shows a three-dimensional collection of transient RIXS spectra for an excitation energy of 402.5 eV. Furthermore, a two dimensional representation is illustrated in Fig. 3. The most dominant overlap of the bleach and excited state RIXS signal can be observed between 30 fs and 60 fs. Furthermore, less significant overlap signals can be found at about 110 fs and 175 fs. However, in each case the excited state features are very weak compared to the bleach signal such that a proper extraction of excited state mechanisms are nearly impossible using this excitation energy. The ground state bleach signal contains five dominant emission bands stemming from six core-to-valence state transitions. Its time-independent pattern is explained in the main article.

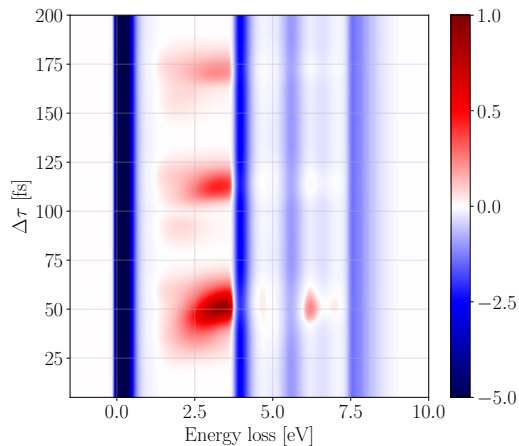


FIG. 2. Three-dimensional collection of calculated difference RIXS spectra for time delays $\Delta\tau$ between 5 fs and 200 fs with a step size of 5 fs using an excitation energies of 402.5 eV.

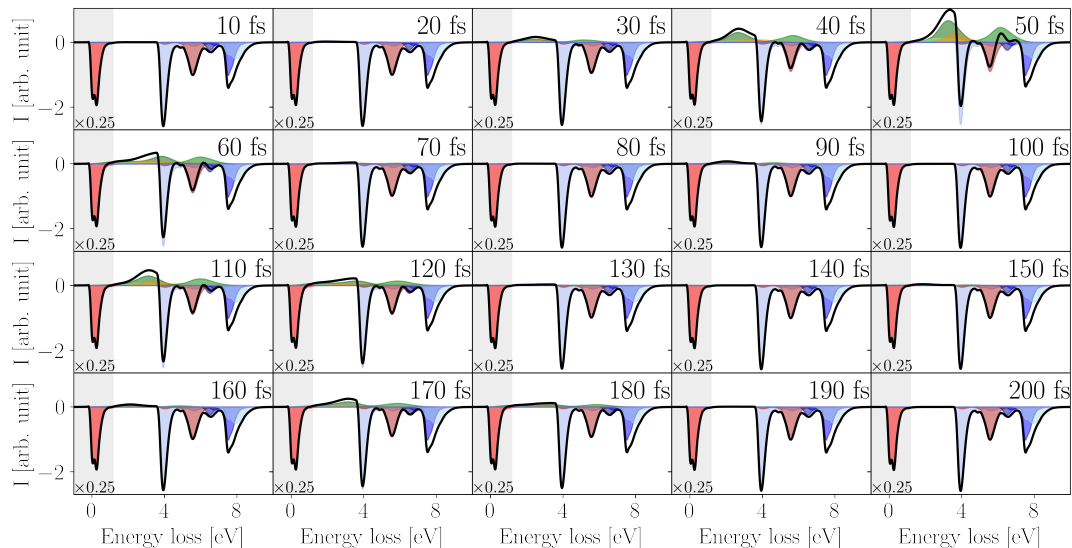


FIG. 3. Time evolution of the difference RIXS spectra between 10 fs and 200 fs with a stepsize of 10 fs steps using an excitation energy of $\omega_I = 402.5$ fs. Transitions stemming from X_1 , X_2 , X_3 and X_4 are highlighted in red, blue, green and yellow, respectively. The elastic peak at 0 eV is downscaled to 25% for a better visualisation.

A two dimensional representation of the time evolution of the transient RIXS spectra computed with excitation energies of 399.0 eV and 401.5 eV are given in Fig. 4 and Fig. 5, respectively. Their behaviour is discussed in the main article.

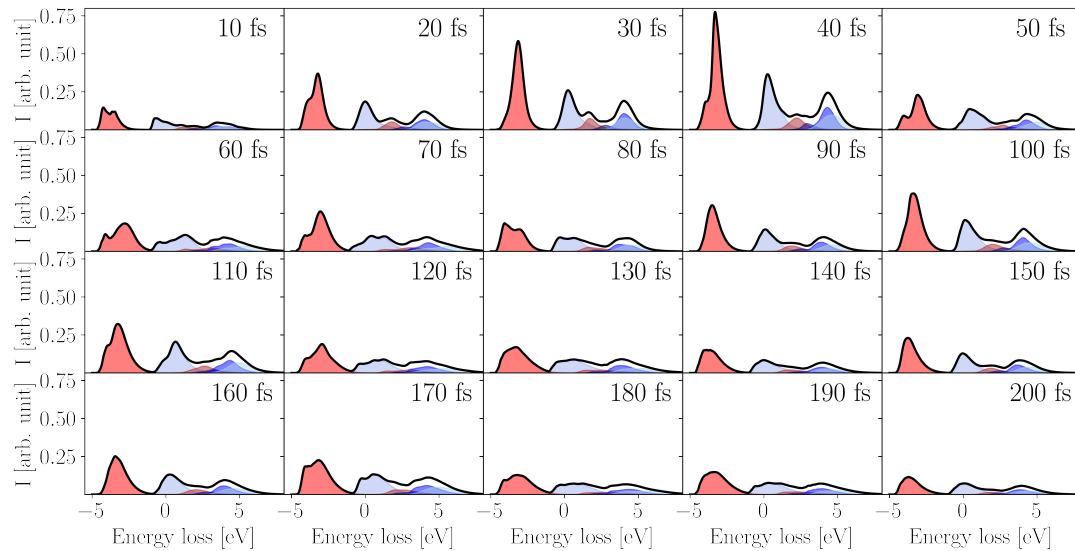


FIG. 4. Time evolution of the RIXS spectra between 10 fs and 200 fs with a stepsize of 10 fs steps using an excitation energy of $\omega_I = 399.0$ fs. Transitions stemming from X_1 and X_2 are highlighted in red and blue, respectively.

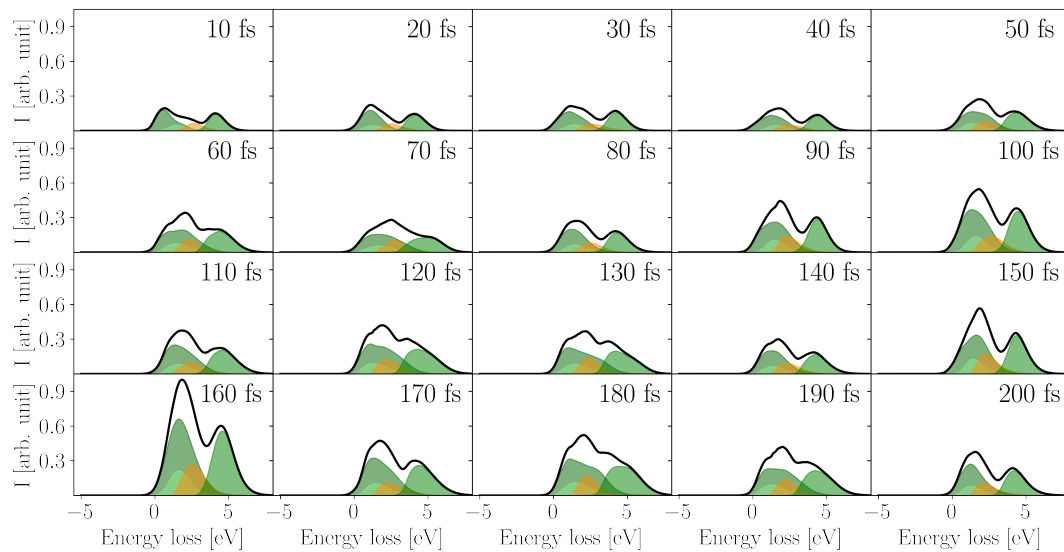


FIG. 5. Time evolution of the RIXS spectra between 10 fs and 200 fs with a stepsize of 10 fs steps using an excitation energy of $\omega_I = 401.5$ fs. Transitions stemming from X_3 and X_4 are highlighted in green and yellow, respectively.

-
- [1] Matthieu Sala, Benjamin Lasorne, Fabien Gatti, and Stéphane Guérin. The role of the low-lying dark $n\pi^*$ states in the photophysics of pyrazine: a quantum dynamics study. *Phys. Chem. Chem. Phys.*, 16:15957–15967, 2014.
 - [2] Antonia Freibert, David Mendive-Tapia, Nils Huse, and Oriol Vendrell. Time-dependent resonant inelastic x-ray scattering of pyrazine at the nitrogen k-edge: A quantum dynamics approach. *Journal of Chemical Theory and Computation*, 20(5):2167–2180, 03 2024.